Supporting Information

Kvajo et al. 10.1073/pnas.1114113108

SI Methods

Expression of Molecules Implicated in Synaptic Plasticity and Excitability. To explore the mechanistic basis of the alterations in frequency facilitation at mossy fiber terminals (MFTs), we performed a quantitative PCR (qRT-PCR) analysis on RNA from the isolated dentate gyrus (DG) (Fig. S6*A*) of several molecules implicated in this form of plasticity. Specifically, we tested the expression of the metabotropic glutamate receptor (mGluR2) (1), the Grik1 (GluR5) kainate receptor (2), the ryanodine receptor (3), and adenylyl cyclase (AC) 8 (4) (Fig. S6 *B*–*E*). Additionally, we tested the protein levels of the kainate receptor Grik5 (KA2) (5) in the isolated CA3 (Fig. S6*F*). Moreover, we performed an analysis of the DG expression of Kcnk1 (Twik-1), a potassium channel that has been implicated in the regulation of granule cell (GC) excitability (Fig. S6*H*) (6). We found no changes in the levels of these candidate genes.

Constructs. Mouse *Disc1* cDNA encoding the L Disc1 isoform was cloned from mouse brain RNA using RT-PCR and verified by sequencing. PCR amplification using a primer with the HA tag sequence was used to generate the C-terminal HA tag on *Disc1*. The amplified fragment was subsequently cloned into the pcDNA3.1 vector (Invitrogen) through XhoI and EcoRI restriction sites. The β-actin–GFP expressing plasmid was described before (7).

Analysis of Dendritic Complexity and Axonal Terminals in *Thy1-GFP* Mice. Mutant *Disc1* mice were crossed with a reporter strain expressing GFP under the *Thy1* promoter (*Thy1-GFP*, line M) (8). The *Thy1-GFP* reporter strain was backcrossed to the C57BL/6J genetic background for nine generations. For all quantifications, postnatal day (P)11 mutant/*Thy1-GFP* mice and their wild-type (WT)/*Thy1-GFP* littermates were perfused and postfixed with 4% paraformaldehyde (PFA); 100-μm coronal vibratome sections were counterstained with the nuclear stain Topro (1:2,500; Invitrogen) and mounted with ProLong Gold (Invitrogen). Dendritic complexity analysis was performed as described (9). For the quantification of MFT distribution, 10× images of the MF were scanned with the confocal microscope [four WT, four heterozygous (HET), and five homozygous (HOM) images; 4–5 sections/mouse]. For the quantification in the proximal MF, the region of interest was defined by drawing one line between the tips of the upper and lower blades of the DG as described (10) and another line from the tip of the distal MF crescent perpendicular to the proximal CA3 cell body layer. The cell body layer (stained with Topro) was then outlined between these two reference lines (Fig. S2 shows a schematic representation). The number of GFP-labeled terminals was counted within, above, and below the cell body layer and expressed as a percentage of the total number of labeled terminals within these regions (to normalize for the variable expression of the *Thy1-GFP* transgene among mice). For the quantification in the distal MF, a line was drawn from the tip of the MF crescent to the proximal CA3 cell body layer. The cell body layer of the distal CA3 demarcated by this line was then outlined, and the terminals within and outside (in the stratum lucidum) the cell body layer were counted and expressed as percentages of the total number of terminals in these regions. Only puncta larger than 4 μm and most likely to represent MFT (11) were included in the analysis.

Rolipram Treatment. Rolipram (1 mg/kg; Sigma) in PBS containing 2% dimethyl sulfoxide or the vehicle alone was administrated to C57BL/6J littermate pups daily from P6 to P11. At P11, mice were perfused with 4% PFA, and the brains were processed for Neuropilin 1 (Nrp1) immunohistochemistry as described below.

Immunohistochemistry. Mice were perfused with PBS and 4% PFA and postfixed in 4% PFA overnight (o/n). For experiments at P11, 5 sections/mouse were quantified, and for adults, 4 sections/mouse were quantified; 40-μm vibratome coronal sections were incubated o/n at 4 °C in the primary antibodies antisynaptophysin (mouse, 1:1,000; Sigma), anticalbindin (rabbit, 1:1,000; Swant), anti–PSA-NCAM (mouse, 1:1,000; Chemicon), anti-cAMP (rabbit, 1:1,000; Chemicon), anti-Nrp1 (goat, 1:1,000; R&D), anti-Sema3a (central region, rabbit, 1:1,000; ECM Biosciences), and anti-NeuN (mouse, 1:1,000; Chemicon) and incubated for 1 h at room temperature with Alexa-conjugated secondary antibodies (1:1,000; Invitrogen) followed by Topro. The length of calbindin-stained MF bundles was measured as described (10). This method was also used to measure the separation of the supra- and infrapyramidal bundles. The line between the end blades was used as a reference point, and the distance at which the bundles separate (i.e., when the bundles are clearly outlined with few distinct crossing fibers between them) was then measured.

Synaptophysin immunoreactivity has been previously used to label and analyze the distribution of MFT in the CA3 (12, 13). Synaptophysin-labeled MFTs can be easily distinguished from other terminals because of their unique size. This distinct property is best appreciated through a comparison of synaptophysin immunoreactivity in the stratum lucidum and the stratum oriens of the distal CA3. MFTs are located exclusively in the stratum lucidum, whereas smaller synaptic terminals are located in the stratum oriens (14) (Fig. S8*A*). Moreover, synaptophysin labeling is restricted to the MFT and not found in MF, making it a specific synaptic marker (Fig. S8*B*).

For Nrp1 immunoreactivity quantification, P11 vibratome sections were labeled against Nrp1 and calbindin and imaged at 20× on a confocal microscope. Sections were loaded into ImageJ software (National Institutes of Health), and the region of interest, which encompassed the entire distal part of the MFs as labeled by calbindin, was selected. The intensity of Nrp1 staining in this region was measured. For the quantification of Semaphorin 3a (Sema3a) immunoreactivity in the CA3, pyramidal neurons were labeled with the anti-Sema3a antibody and the neuronal marker NeuN, which labels the pyramidal cell layer. A region of interest encompassing the whole distal CA3, as outlined by NeuN, was selected. For the quantification of cAMP immunoreactivity in the DG, we used an antibody that was previously used for cAMP quantification analysis (15–18). The GC layer was visualized using Topro, and a region of interest in the central part of the upper blade was selected. cAMP immunoreactivity was observed as punctate as well as diffuse cytoplasmic staining. It has been speculated that the punctuate staining may represent pools of cAMP associated with protein kinase A subunits (19). The ImageJ program was used to separately quantify the punctuate and cytoplasmic pool of cAMP. Results from the cytoplasmic pool only are shown in Fig. 6*L*, but analysis of both fractions also confirms the increase in cAMP levels in the DG of *Disc1* mutant mice.

Nissl Staining. Forty-micrometer vibratome sections were stained with a mixture of cresyl violet and neutral red as previously described (9).

Retroviral Labeling and Analysis of Adult-Born Neurons. Adult-generated DG neurons were labeled with a replication-defective

Moloney murine leukemia virus (MMLV) that infects dividing neural progenitors and expresses GFP under control of the strong ubiquitous CAG synthetic promoter. GFP-expressing MMLV retrovirus pseudotyped with the vesicular stomatitis virus glycoprotein (VSV-G) coat protein was produced by transfection of the pCL-CAG:eGFP vector plasmid (a kind gift from Inder Verma, Salk Institute, San Diego, CA) along with gag-pol and VSV-G packaging plasmids into the HEK293FT packaging cell line with Lipofectamine 2000 (Invitrogen). After harvesting the viral supernatant, virus was concentrated through ultracentrifugation to a final titer of 10^9 cfu/mL. Adult *Disc1* mice were group housed in an enrichment cage with a running wheel for 1 d before injection. Mice were injected with a mixture of ketamine and xylazine (100 and 10 mg/kg, respectively), and then, they were injected bilaterally using a mouse sterotactic apparatus (Stoelting) using a microinfusion pump (Stoelting) with 0.5 μL virus per site at a speed of 0.1 μL/min into the DG at these coordinates [anterior-posterior (AP), −2.0; mediolateral (ML), ±1.5; dorsal-ventral (DV), −2.1]. Mice were allowed to recover and then put back into the enrichment cages for a period of 1 (five WT, five HET, and five HOM mice), 2 (five WT, six HET, and five HOM mice), or 4 wk (six WT, five HET, and six HOM mice). Mice were then perfused with PBS followed by 4% PFA. Brains were postfixed overnight in PFA, and 100-μm vibratome coronal sections were stained for GFP (rabbit, 1:1,000; Invitrogen) and counterstained with Topro. Dendritic tree morphology was analyzed as described (9). Cell soma size was determined by outlining the soma followed by automatic calculation of area in micrometers squared. Proximal dendritic spines were counted starting from the first branch point over a distance of 50 μm. For distal dendritic spines, the number of spines within a 50-μm span starting from the tip of a dendrite was counted. The length of the longest axon was quantified as described (10). The quantification of the axonal distribution in the proximal CA3 was done essentially as for the P11 Thy1/GFP mice. The number of axonal protrusions was quantified above, below, and within the cell body area and expressed as a percentage.

Electrophysiology. All experimental mice were male littermates (6–8 wk for field recordings and 4–6 wk for whole-cell recordings). Mice were anesthetized with isoflourane and then decapitated. The brain was removed and chilled in ice-cold dissection solution (195 mM sucrose, 10 mM NaCl, 2.5 mM KCl, 1 mM NaH_2PO_4, 25 mM $NaHCO_3$, 10 mM glucose, 5 mM $MgCl_2$, 1 mM $MgSO_4$, 0.5 mM $CaCl_2$) and 400-μm sections were cut on a vibratome (VT1200S; Leica). For field recordings, the hippocampus (HPC) was dissected from the brain and cut transversely. Slices were immediately transferred to an interface chamber and allowed to recover for at least 2 h at 31–32 °C. For whole-cell recordings, horizontal brain slices were cut and recovered in a submerged chamber at 37 °C for 1 h and then, room temperature until use in artificial cerebrospinal fluid (ACSF) (124 mM NaCl, 2.5 mM KCl, 1 mM NaH_2PO_4, 25 mM $NaHCO_3$, 10 mM glucose, 1 mM $MgSO_4$, 2 mM $CaCl_2$).

Extracellular field recordings were made in an interface chamber (Fine Science Tools) at 31–32 °C in ACSF (2 mL/min) with a recording electrode (<2 MΩ) filled with ACSF. Stimulation was with a concentric bipolar stimulating electrode (tip diameter = 0.125 mm; FHC). Data were acquired by pClamp10 software using an extracellular amplifier (ER-1; Cygnus Technolgies) and Axon Instruments Digidata 1440A. To record MF input to CA3 pyramidal neurons, the recording electrode was placed in stratum lucidum of CA3, and the GC layer of the DG was stimulated. MF input was confirmed by a 1-Hz frequency facilitation >375% and 50-ms paired-pulse facilitation >2.4. In a subset of experiments from all genotypes the group 2 mGluR agonist DCGIV (1 μM) was applied at the end of the experiment. Whenever frequency facilitation was >375%, this compound reduced evoked excitatory postsynaptic potential (eEPSP) amplitude by >85% (20). The amplitude was taken as the magnitude of the evoked EPSP. For LTP studies, test stimuli were delivered at one-half the maximal size, and tetani were delivered at this intensity; 20- to 30-min baselines were recorded, and data were normalized to the final 10 min. LTP was induced by two trains of 1 s at 100 Hz (21) separated by 30-s intervals. For MF short-term plasticity experiments, stimulation was at one-half the maximum.

Whole-cell patch clamp recordings were made at 31–32°C in the same ACSF using boroscillate glass pipettes (initial resistance = 4–5 MΩ) containing an internal solution of 130 mM $KMeSO_4$, 10 mM KCl, 10 mM Hepes, 4 mM NaCl, 0.1 mM EGTA, 4 mM MgATP, 0.3 mM Na_2GTP, 10 mM phosphocreatine. Junction potentials were not corrected. Input resistance was calculated as the slope of membrane polarization in response to current injection −50 to +25 pA at resting potential. Mature GCs, unlike immature neurons, sit at very polarized potentials (22, 23) and fire trains of action potentials (24). Therefore, to compare equivalent populations, only neurons with resting potentials negative to −65 mV and firing trains were included in our analysis, which represented 81% of WT neurons and 79% of HOM neurons. Data were analyzed using Clampfit, Sigmaplot, and Sigmastat software.

Measurement of cAMP in Hippocampal Homogenates. For cAMP measurement, HPC was homogenized in ice-cold 0.1 N hydrochloric acid and centrifuged at 13,000 × *g* for 50 min at 4 °C. cAMP in the supernatant was measured by ELISA according to manufacturer's instructions (Assay Designs); 5 mice/genotype were used.

Phosphodiesterase Activity Assay. The phosphodiesterase (PDE) activity assay was performed on dissected HPC as described (25). Samples were assayed in the presence or absence of 10 μM rolipram. PDE4 activity (i.e., rolipram sensitivity) was calculated by subtracting cAMP hydrolysis in the presence of rolipram from cAMP hydrolysis in its absence; 4 mice/genotype were used.

Radioligand Binding Assays. [^{3}H] rolipram binding was measured as described previously (26). HPC lysate samples containing 200 μg protein were incubated at 30 °C in the presence of 250 μL incubation buffer that contains different concentrations of [^{3}H] rolipram (2–30 nM). Nonspecific binding was determined in the presence of 10 nM unlabeled 4-(3-butoxy-4-methoxybenzyl)-2-imidazolidinone (Ro 20–1724) for [^{3}H] rolipram binding. Reactions were stopped by the addition of 5 mL ice-cold binding buffer after 1 h and were followed by rapid vacuum filtration through glass fiber filters. The filters were washed two times, and radioactivity was measured by liquid scintillation counting.

Real-Time qRT-PCR Analysis. DG from adult mice was dissected out as described (27) and placed o/n in RNAlater (Ambion). RNA was then isolated using RNeasy (Qiagen). Approximately 2 μg total RNA were reverse-transcribed into double-stranded cDNA and then diluted 1:10 in ddH_2O. Expression levels were assessed by TaqMan Gene Expression Assays: Mm00435379_m1 (Nrp1), Mm00803099_m1 (Nrp2), Mm00501170_m1 (Plxna3), Mm00451266_m1 (Tdo2), Mm00434624_m1 (Twik-1), Mm00507722_m1 (Adcy 8), Mm01235831_m1 (mGluR2), Mm01175211_m1 (RyR1), and Mm00446882_m1 (GluR5). Expression of TaqMan mouse Gapdh probe (Applied Biosystems) was used for normalization. qRT-PCR was run as a 14-μL reaction of 7 μL 2× TaqMan Universal Master Mix (Applied Biosystems), 0.25 μL Gapdh probe, 0.5–2 μL probe of interest, and 1.6 μL cDNA using five technical repeats per cDNA sample on an ABI 7900HT Real-Time PCR system (Applied Biosystems). Pooled cDNA was used to generate a dilution series run in duplicate on each plate for expression quantification. Cycle thresholds were determined using SDS 2.3 software (Applied Biosystems). Expression data were calculated using median values for ddCt and standard curve formulas (www.AppliedBiosystems.com) and normalized to the average of WT values. To verify the specificity of

DG dissection, DG and Ammon horn from five WT mice were dissected out, and the expression of Tdo2, a DG-specific marker, was determined (27).

For the quantification of PDE4b expression, total RNA was isolated from HPC with TRIzol reagent (Invitrogen) according to manufacturer's instruction and followed by DNase treatment to eliminate contaminated genomic DNA. Conversion of total RNA into cDNA was performed using the High-Capacity cDNA Archive Kit (Applied Biosystems). Real-time PCR was performed on an ABI PRISM 7300 Detection System (Applied Biosystems) with Taqman Universal Mastermix (Applied Biosystems). The PDE4B primer was purchased from Applied Biosystems. The samples were run in triplicate and amplified for 40 cycles (50 °C for 2 min, 90 °C for 10 min, 95 °C for 15 s, and extension 60 °C for 1 min). β-Actin was used as an endogenous control. The fold difference in expression of target cDNA was determined using the comparative threshold method as previously described (28). Statistical analysis was performed using one-way ANOVA followed by Dunnett's test; three mice per genotype were used.

Immunoblotting. To determine phospho-CREB levels, HPC (5 mice/genotype) was homogenized in ice-cold lysis buffer (Upstate) and centrifuged at 10,000 × *g* for 30 min at 4 °C. Solubilized samples were mixed with equal volumes of Laemmli sample buffer and heated to 100 °C for 2 min. Equal amounts of sample protein were loaded onto gels for SDS/PAGE. After separation by electrophoresis, proteins in the gels were transferred to nitrocellulose membranes, which were incubated overnight at 4 °C with primary antibodies against CREB phosphorylated at serine-133 (Upstate Biotechnology) or PDE4A, -B, or -D (4 mice/genotype; FabGennix). This process was followed by incubation with Alexa Fluor 680-conjugated secondary antibody for 30 min at room temperature (Invitrogen). An Odyssey Infrared Imaging System (LI-COR Bioscience) was used for quantifying fluorescence.

For protein analysis in the CA3, brains from adult mice were rapidly dissected out and cut to 1-mm-thick coronal sections. Sections were then briefly stained in 0.3% methylene blue diluted in cold PBS to outline the pyramidal cell layer of the CA3. The CA3 region was then dissected out, and crude synaptosomal preparations were made by homogenizing in 100 μL buffer containing 5 mM Hepes/10% sucrose (pH 7.5). Homogenates were spun down at 1000 × *g*, and the supernatant was further centrifuged at 12,000 × *g*. The pellet was resuspended in the same buffer, and 10 μg protein were analyzed by Western blotting. After the transfer, nitrocellulose membranes were probed with an antibody raised against the N-terminal domain of Disc1 (29) and the anti-synaptophysin antibody (mouse, 1:2,000; Sigma) or with a rabbit anti-KA2 antibody (1:1,000; Millipore) and an anti–α-tubulin antibody (1:100,000; Sigma).

Primary Cell Cultures, Transfection, and Treatment. E17.5 hippocampal neurons were dissociated enzymatically (0.25% trypsin, DNase), mechanically triturated, and plated on 35-mm dishes (4×10^5 hippocampal cells/dish) with glass coverslips coated with poly-DL-ornithine (Sigma) in DMEM (Invitrogen) supplemented with 10% FBS (Invitrogen). Four hours after plating, DMEM was replaced by Neurobasal medium (Invitrogen) supplemented with 2 mM glutamine and 2% B27 (Invitrogen). For dendritic analyses, primary cultures were transfected after 2 d in culture (DIV2) and analyzed on day 5 (DIV5). Cells were transfected with constructs using Lipofectamine and Plus-Reagent (Invitrogen) as described by the manufacturer (Invitrogen). Neurite analysis was carried out with ImageJ software (National Institutes of Health). For the quantification of cAMP levels, neurons from all three genotypes were stained as described (15) using the rabbit anti-cAMP antibody (Chemicon) and counterstained with the mouse anti-Tau1 antibody (1:5,000, Chemicon). Tau1 is enriched in axons but also labels the cell bodies of developing neurons in culture (30). Images of individual neurons were obtained using confocal microscopy, and signal intensity within the cell body area and growth cones was quantified using ImageJ software. For the inhibition of adenyl cyclase, DIV2 neurons were transfected with GFP, and 24 h later, SQ-22536 (Sigma) was added to the cell culture medium at the final concentration of 100 μM. After another 25 h, cells were fixed, and their dendritic complexity was determined. The carpets for the stripe assays were prepared as described (31). Hippocampal neurons of all three genotypes were plated on individual carpets and after 48 h, fixed and stained for Tau1. For the analysis, 10× confocal images were acquired starting from one end of the carpet until reaching the other end (typically 10 images). The repulsion of neurites was quantified as described (32). Neurons were scored as nonrepulsed if their neurites at any point entered the Ephrin-A5–containing stripes and calculated as a percentage of the total number of neurons. Only neurons with cell bodies localized on the control stripes were analyzed. For the rescue experiments, 10 μm SQ-22536 were added to the cell medium 4 h after plating and again after 20 h; 24 h later, cells were fixed and analyzed.

DG Explant Culture. DG explant culture was prepared as described (33). For the treatment, SQ-22536 (final concentration of 10 μM) was added to the culture medium 4 h after plating, and replenished after 20 h; 48 h after plating, explants were fixed and processed for Nrp1 (1:1,000) and Gap43 (1:1,000; Invitrogen) immunocytochemistry. For the quantification, images of growth cones were loaded onto ImageJ, and analysis of the intensity was performed.

EM. Adult mice were perfused with PBS and 4% glutaraldehyde in PBS. Brains were postfixed overnight in the same solution and then cut at 60 μm on a vibratome. Using microwave methods for EM, sections were postfixed in 1% osmium tetroxide and then dehydrated in an ethanol series of 50%, 70%, 95%, and 2× 100%. Sections were then infiltrated with a 1:1 mixture of 100% epon and 100% ethanol and then infiltrated in 100% epon two times. Sections were then mounted between plastic slides with 100% epon and polymerized overnight at 60 °C. The next day, the polymerized epon wafers with sections were separated from the plastic slides, and the area of interest was cut from the section and remounted on a blank epon stub. Once remounted, the area of interest was trimmed for sectioning and collected on formvar-coated slot grids. The serial sections on slot grids were then stained with uranyl acetate and lead citrate and examined on a JEOL 1200EX electron microscope. Axon terminals were studied ultrastructurally using 30,000× and 75,000× magnifications, with a focus on the mature boutons, which are characterized by their large size, large number of synaptic vesicles, and presence of multiple synaptic contacts with organelles-containing dendritic spines (34); 30,000× images were analyzed in the Reconstruct program (35) to determine area of the boutons, the number and size of spines that contact the presynaptic bouton, and the number and size of active zones (36). The 75,000× images were used to determine the density of vesicles in the center of the bouton. A region of interest was chosen using the rectangle tool in the Reconstruct program. The number of small clear vesicles was then determined. The diameter of a randomly chosen subset of the clear core vesicles was measured using the line tool, and this length was used to determine the volume of individual vesicles [$V = 4/3\pi\ (d/2)^3$]. Five WT, four HET, and five HOM mice were analyzed.

Statistical Analysis. One-way ANOVA (as implemented in GraphPad) was used except for the analysis of terminal distribution in the proximal and distal CA3, where the interaction of genotype and region was analyzed using two-way ANOVA. The Kolmogorov–Smirnov test was used for the analysis of MFT vesicle size distribution. For the comparisons of frequency facilitation in

response to trains of stimuli, changes in maximal frequency facilitation vs. stimulation frequency, spiking rates in response to an incremental series of current injections, and interspike intervals over the course of 10-action potential trains were made using a two-way, repeated measures ANOVA; all other comparisons used a *t* test.

1. Yokoi M, et al. (1996) Impairment of hippocampal mossy fiber LTD in mice lacking mGluR2. *Science* 273:645–647.
2. Lauri SE, et al. (2001) Synaptic activation of a presynaptic kainate receptor facilitates AMPA receptor-mediated synaptic transmission at hippocampal mossy fibre synapses. *Neuropharmacology* 41:907–915.
3. Lauri SE, et al. (2003) A role for Ca2+ stores in kainate receptor-dependent synaptic facilitation and LTP at mossy fiber synapses in the hippocampus. *Neuron* 39:327–341.
4. Wang H, et al. (2003) Type 8 adenylyl cyclase is targeted to excitatory synapses and required for mossy fiber long-term potentiation. *J Neurosci* 23:9710–9718.
5. Breustedt J, Schmitz D (2004) Assessing the role of GLUK5 and GLUK6 at hippocampal mossy fiber synapses. *J Neurosci* 24:10093–10098.
6. Young CC, et al. (2009) Upregulation of inward rectifier K+ (Kir2) channels in dentate gyrus granule cells in temporal lobe epilepsy. *J Physiol* 587:4213–4233.
7. Mukai J, et al. (2004) Evidence that the gene encoding ZDHHC8 contributes to the risk of schizophrenia. *Nat Genet* 36:725–731.
8. Feng G, et al. (2000) Imaging neuronal subsets in transgenic mice expressing multiple spectral variants of GFP. *Neuron* 28:41–51.
9. Kvajo M, et al. (2008) A mutation in mouse Disc1 that models a schizophrenia risk allele leads to specific alterations in neuronal architecture and cognition. *Proc Natl Acad Sci USA* 105:7076–7081.
10. Zhao C, Teng EM, Summers RG, Jr., Ming GL, Gage FH (2006) Distinct morphological stages of dentate granule neuron maturation in the adult mouse hippocampus. *J Neurosci* 26:3–11.
11. Danzer SC, He X, Loepke AW, McNamara JO (2010) Structural plasticity of dentate granule cell mossy fibers during the development of limbic epilepsy. *Hippocampus* 20: 113–124.
12. Heyden A, Angenstein F, Sallaz M, Seidenbecher C, Montag D (2008) Abnormal axonal guidance and brain anatomy in mouse mutants for the cell recognition molecules close homolog of L1 and NgCAM-related cell adhesion molecule. *Neuroscience* 155:221–233.
13. Montag-Sallaz M, Schachner M, Montag D (2002) Misguided axonal projections, neural cell adhesion molecule 180 mRNA upregulation, and altered behavior in mice deficient for the close homolog of L1. *Mol Cell Biol* 22:7967–7981.
14. Ishizuka N, Weber J, Amaral DG (1990) Organization of intrahippocampal projections originating from CA3 pyramidal cells in the rat. *J Comp Neurol* 295:580–623.
15. Yamada RX, Matsuki N, Ikegaya Y (2005) cAMP differentially regulates axonal and dendritic development of dentate granule cells. *J Biol Chem* 280:38020–38028.
16. Trousse F, Martí E, Gruss P, Torres M, Bovolenta P (2001) Control of retinal ganglion cell axon growth: A new role for Sonic hedgehog. *Development* 128:3927–3936.
17. He YL, Zhan XQ, Yang G, Sun J, Mei YA (2010) Amoxapine inhibits the delayed rectifier outward K+ current in mouse cortical neurons via cAMP/protein kinase A pathways. *J Pharmacol Exp Ther* 332:437–445.
18. Bouchard JF, et al. (2004) Protein kinase A activation promotes plasma membrane insertion of DCC from an intracellular pool: A novel mechanism regulating commissural axon extension. *J Neurosci* 24:3040–3050.
19. Wiemelt AP, Engleka MJ, Skorupa AF, McMorris FA (1997) Immunochemical visualization and quantitation of cyclic AMP in single cells. *J Biol Chem* 272: 31489–31495.
20. Kamiya H, Shinozaki H, Yamamoto C (1996) Activation of metabotropic glutamate receptor type 2/3 suppresses transmission at rat hippocampal mossy fibre synapses. *J Physiol* 493:447–455.
21. Zalutsky RA, Nicoll RA (1990) Comparison of two forms of long-term potentiation in single hippocampal neurons. *Science* 248:1619–1624.
22. Spruston N, Johnston D (1992) Perforated patch-clamp analysis of the passive membrane properties of three classes of hippocampal neurons. *J Neurophysiol* 67:508–529.
23. Staley KJ, Otis TS, Mody I (1992) Membrane properties of dentate gyrus granule cells: Comparison of sharp microelectrode and whole-cell recordings. *J Neurophysiol* 67: 1346–1358.
24. Schmidt-Hieber C, Jonas P, Bischofberger J (2004) Enhanced synaptic plasticity in newly generated granule cells of the adult hippocampus. *Nature* 429:184–187.
25. Zhang HT, et al. (2006) Antidepressant-like effects of PDE4 inhibitors mediated by the high-affinity rolipram binding state (HARBS) of the phosphodiesterase-4 enzyme (PDE4) in rats. *Psychopharmacology (Berl)* 186:209–217.
26. Zhao Y, Zhang HT, O'Donnell JM (2003) Antidepressant-induced increase in high-affinity rolipram binding sites in rat brain: Dependence on noradrenergic and serotonergic function. *J Pharmacol Exp Ther* 307:246–253.
27. Hagihara H, Toyama K, Yamasaki N, Miyakawa T (2009) Dissection of hippocampal dentate gyrus from adult mouse. *J Vis Exp* 33:1543.
28. Livak KJ, Schmittgen TD (2001) Analysis of relative gene expression data using real-time quantitative PCR and the 2(-Delta Delta C(T)) method. *Methods* 25:402–408.
29. Koike H, Arguello PA, Kvajo M, Karayiorgou M, Gogos JA (2006) Disc1 is mutated in the 129S6/SvEv strain and modulates working memory in mice. *Proc Natl Acad Sci USA* 103:3693–3697.
30. Dotti CG, Banker GA, Binder LI (1987) The expression and distribution of the microtubule-associated proteins tau and microtubule-associated protein 2 in hippocampal neurons in the rat in situ and in cell culture. *Neuroscience* 23:121–130.
31. Knöll B, Weinl C, Nordheim A, Bonhoeffer F (2007) Stripe assay to examine axonal guidance and cell migration. *Nat Protoc* 2:1216–1224.
32. Knöll B, et al. (2006) Serum response factor controls neuronal circuit assembly in the hippocampus. *Nat Neurosci* 9:195–204.
33. Tawarayama H, Yoshida Y, Suto F, Mitchell KJ, Fujisawa H (2010) Roles of semaphorin-6B and plexin-A2 in lamina-restricted projection of hippocampal mossy fibers. *J Neurosci* 30:7049–7060.
34. Amaral DG, Dent JA (1981) Development of the mossy fibers of the dentate gyrus: I. A light and electron microscopic study of the mossy fibers and their expansions. *J Comp Neurol* 195:51–86.
35. Fiala JC (2005) Reconstruct: A free. for serial section microscopy. *J Microsc* 218:52–61.
36. Otal R, Martínez A, Soriano E (2005) Lack of TrkB and TrkC signaling alters the synaptogenesis and maturation of mossy fiber terminals in the hippocampus. *Cell Tissue Res* 319:349–358.

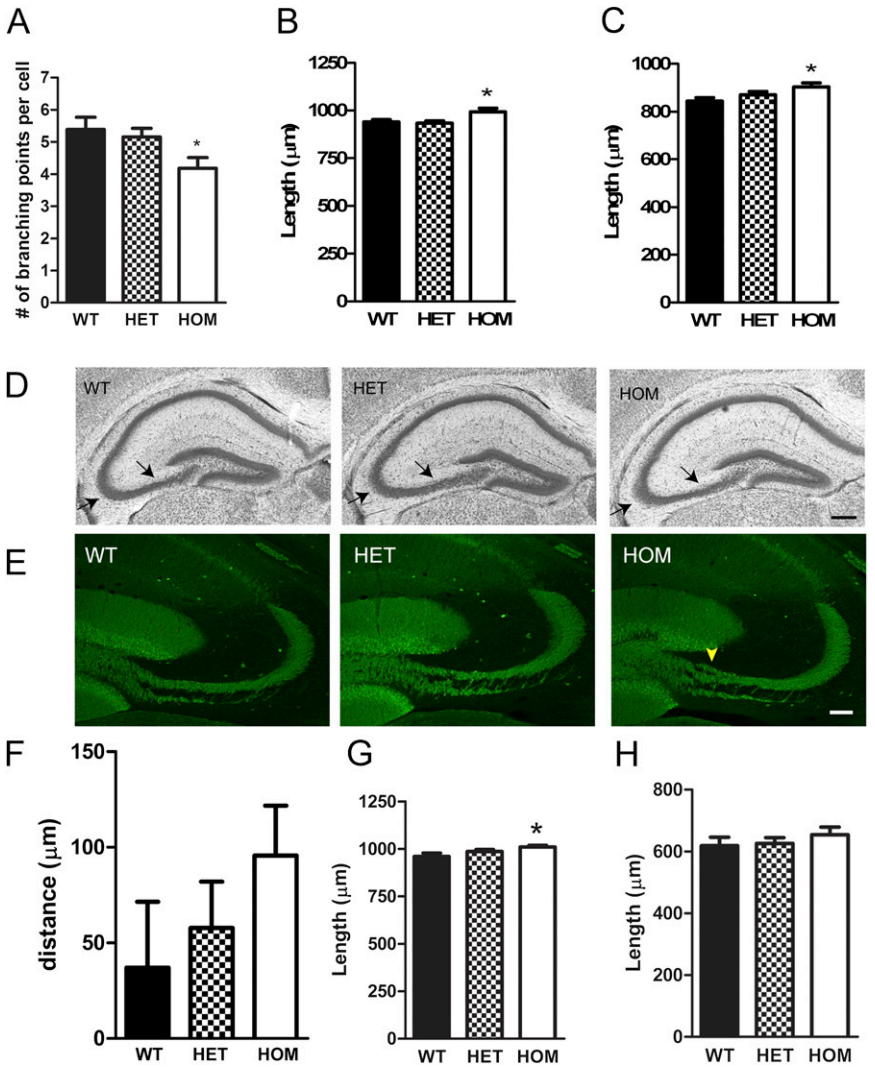

Fig. S1. Granule cell (GC) dendritic complexity and MF projections. (*A*) Dendritic branching points in P11 neurons ($P = 0.017$; $n = 26$, 28, and 28 cells). (*B* and *C*) Increased length of the suprapyramidal (SPB; *B*) and infrapyramidal (IPB; *C*) bundle in P11 mice (SPB: $P = 0.018$, IPB: $P = 0.022$; $n = 6$ mice/genotype). (*D*) Nissl staining of P11 coronal brain sections showing normal gross morphology of the hippocampal formation, including CA3 (arrows). (*E*) Altered bundling in adult HOM mice is indicated by arrowhead. (*F*) Quantification (in micrometers) of the point of IPB and SPB separation ($P = 0.37$; $n = 5$ mice/genotype). (*G* and *H*) Increased length in the SPB (*G*; $P = 0.033$) but not IPB (*H*; $P = 0.55$) in adult mice. (Scale bar: *D*, 200 μm; *E*, 100 μm.)

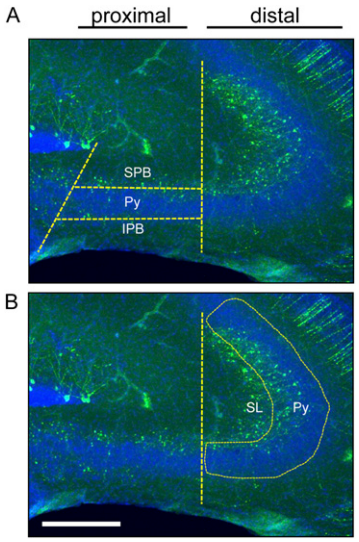

Fig. S2. Regions of interest for the analysis of MFT distribution. (*A* and *B*) Depiction of the regions of interest for the quantification of MFT distribution in the proximal (*A*) and distal (*B*) CA3. The regions of interest are marked with yellow dashed lines. The quantification of terminal distribution was performed as described in *SI Methods*. In the proximal CA3, terminals were quantified within, above, and below the cell body layer (Py); in the distal CA3, they were quantified within the cell body layer (Py) and in the stratum lucidum (SL). (Scale bar: 200 μm.)

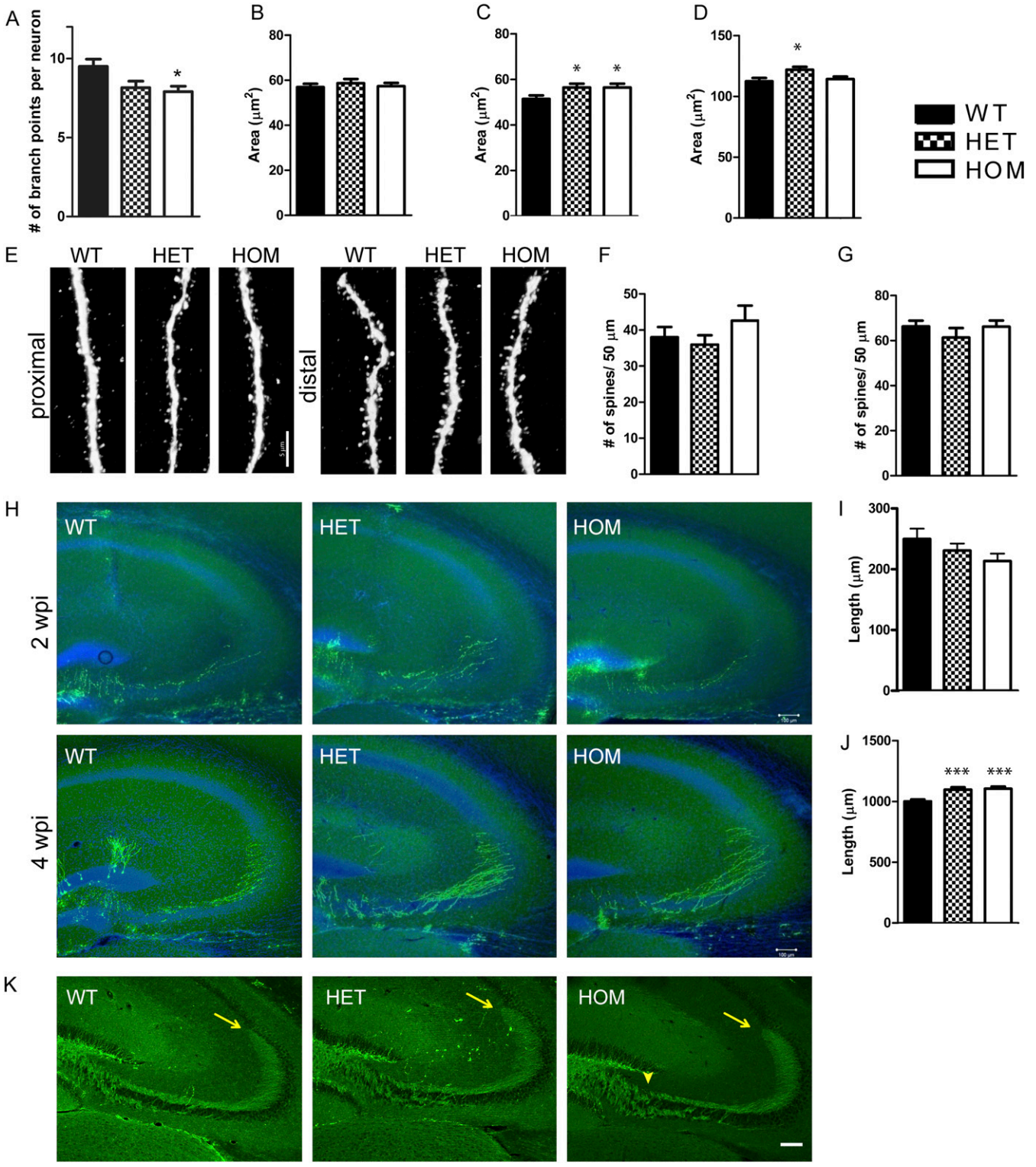

Fig. S3. Analysis of dendritic complexity, soma size, dendritic spine density, and axonal projections of adult-born neurons. (*A*) Number of branch points at 4 wk post injection (wpi; $P = 0.015$; $n = 20$, 19, and 22 cells). (*B–D*) Quantification of cell soma area (in micrometers squared) at 1 (*B*; $P = 0.72$; $n = 68$, 42, and 44 cells), 2 (*C*; $P = 0.047$; $n = 68$, 52, and 44 cells), and 4 wpi (*D*; $P = 0.015$; $n = 80$, 84, and 107 cells). (*E–G*) Representative images of spine density of 4 wpi adult-born neurons at proximal and distal dendrites (*E*). Quantification of spine density at proximal (*F*; $P = 0.34$; $n = 18$, 18, and 14 cells) and distal (*G*; $P = 0.5$) dendrites ($n =$ 16, 10, and 17 cells). (*H* and *I*) Representative images of axonal outgrowth at 2 wpi (*H*) and quantification of axonal length (in micrometers) at 2 wpi (*I*; $P = 0.27$; $n = 14$, 24, and 20 axons). (*H* and *J*) Axonal outgrowth at 4 wpi (*H*) and quantification of axonal length (in micrometers) at 4 wpi (*J*; $P < 0.0001$; $n = 32$, 29, and 27 axons). (*K*) PSA-NCAM staining of axonal projections from 1- to 3-wk-old adult-born neurons. Arrows indicate no overt mistargeting to the CA2/CA1 subfields in either genotype. Arrowhead indicates altered fasciculation in the HOM mice. Values represent mean ± SEM. (Scale bar: *E*, 5 μm; *H* and *K*, 100 μm.)

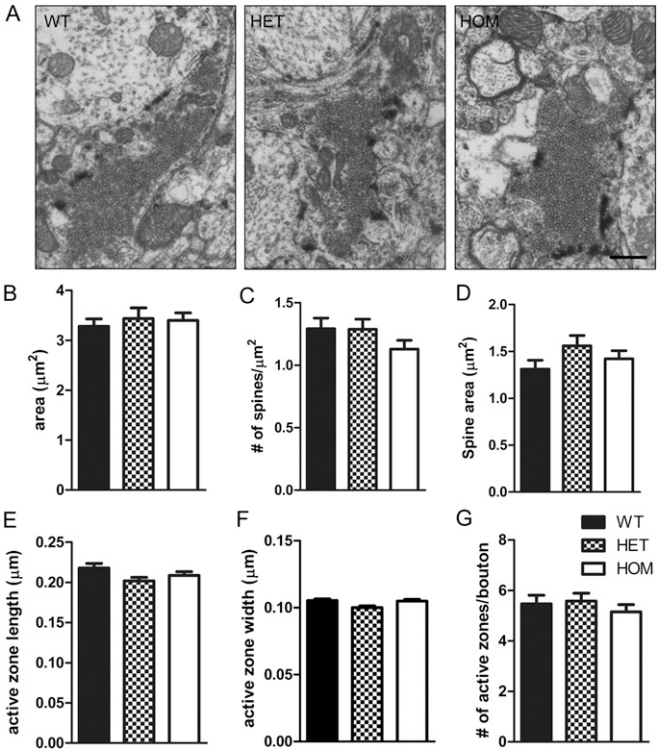

Fig. S4. Electron microscopical analysis of MFT. (*A*–*G*) EM micrographs of MFT from the three genotypes (*A*). (*B*–*G*) Quantification of (*B*) MFT area (n = 76, 64, and 96 terminals), (*C*) number of spines per MFT (n = 76, 64, and 96 terminals), (*D*) spine area (n = 76, 66, and 96 spines), (*E*) active zone length, (*F*) active zone width (n = 415, 556, and 499 active zones), and (*G*) number of active zones per MFT (n = 76, 64, and 96 terminals). Values represent mean ± SEM. (Scale bar: *A*, 500 nm.)

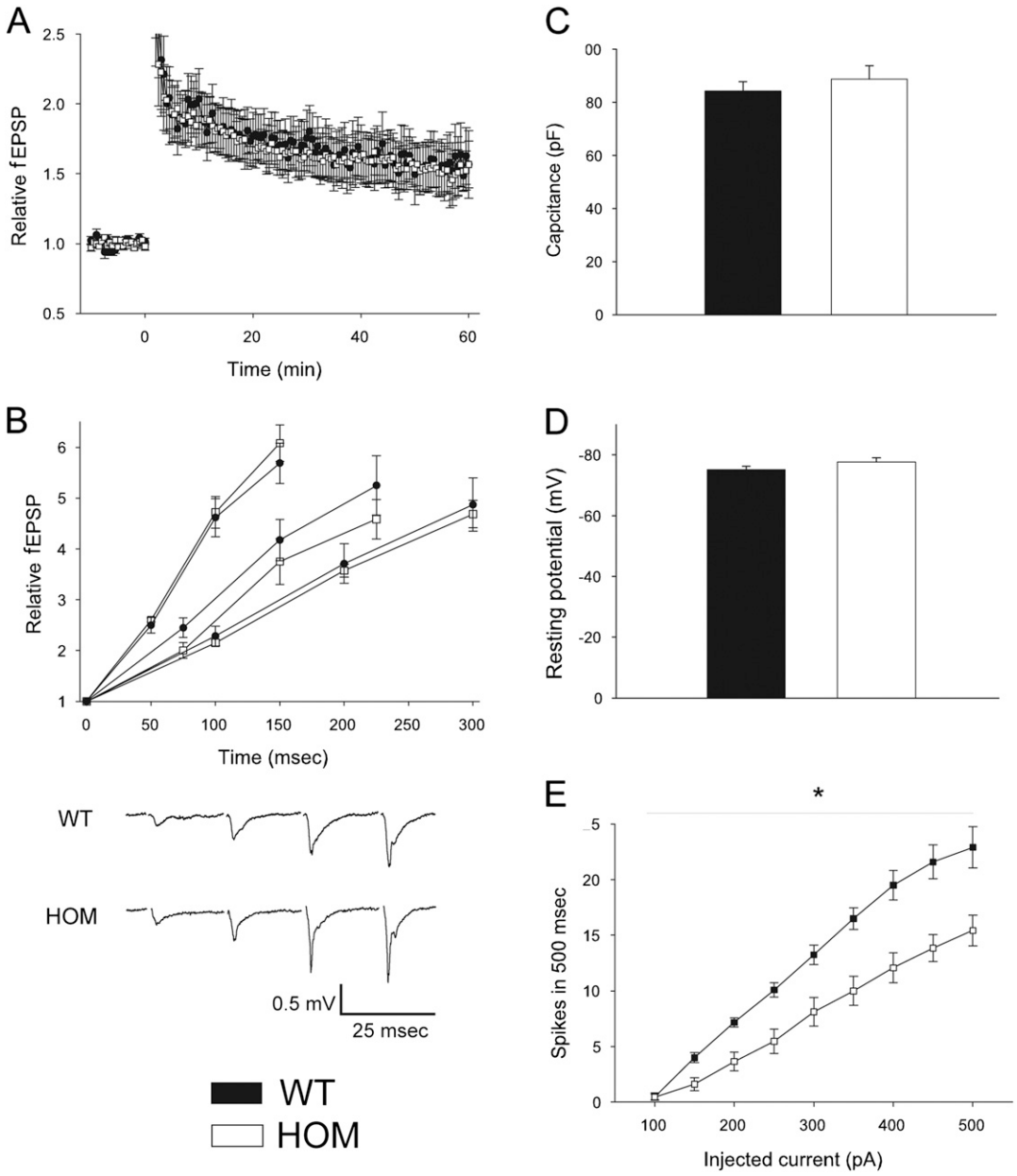

Fig. S5. MF and granule cell recordings. (*A*) LTP of MF inputs to CA3; shown is the data in Fig. 4*F* on an expanded *y* axis scale for clarity. (*B*) Facilitation when the DG was stimulated four times with interstimulus intervals of 50, 75, and 100 ms was not different between genotypes. Below are example traces with a 50-ms interstimulus interval. (Scale bar: *y*, 0.5 mV; *x*, 25 ms.) (*C*) The average capacitance of GCs was not different between genotypes ($P = 0.46$). (*D*) The average resting potential of GCs was not different between genotypes. (*E*) Current was tonically injected into granule cells so that they sat at −80 mV, and then, 500-ms square wave currents were injected at 50-pA increments. Significantly fewer action potentials were evoked in HOM than in WT neurons ($n = 12$ and 6 neurons, respectively; two-way repeated measures ANOVA; effect of genotype: $P = 0.03$, genotype by current injected interaction: $P < 0.001$).

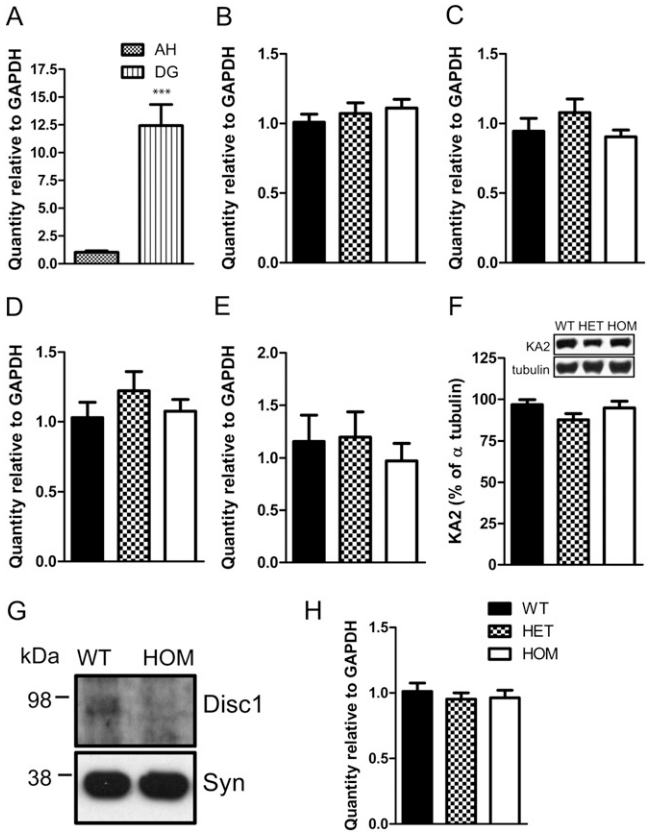

Fig. S6. Expression analysis of molecules implicated in frequency facilitation and granule cell excitability in the DG and the CA3. (*A*) qRT-PCR quantification of TDO2 expression in the dentate gyrus (DG) and Ammon's horn (AH) of WT mice. TDO2 is primarily expressed in the DG, thus showing the specificity of the DG dissection (n = 5 mice). (*B–F*) qRT-PCR analysis of mGluR2 (*B*), Grik1 (GluR5; *C*), RyR1 (*D*), and AC8 (*E*) in the DG and analysis of Grik5 (KA2) levels (*F*) in the CA3 region by Western blotting. (*G*) Immunoblot analysis of crude synaptosomal fractions from the CA3 region of WT and HOM mice with the anti-Disc1 antibody. Synaptophysin (syn) was used as a loading control. (*H*) KCNK1 (TWIK1) expression in the DG. Values represent mean ± SEM. ***$P < 0.0005$.

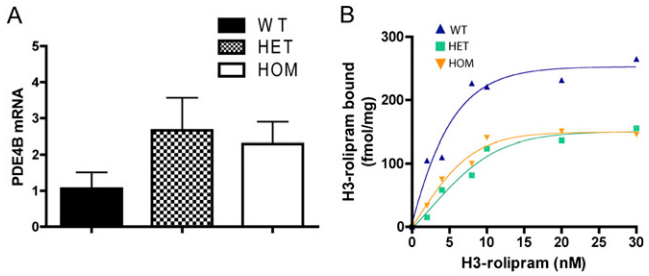

Fig. S7. PDE4B expression levels and rolipram binding. (*A*) PDE4B mRNA levels in the HPC by qRT-PCR. No difference among genotypes was observed (n = 3 mice/genotype). (*B*) Rolipram binding in the HPC of *Disc1*^{Tm1Kara} mice. B_{max} values are decreased in HOM and HET mice (n = 7 mice/genotype).

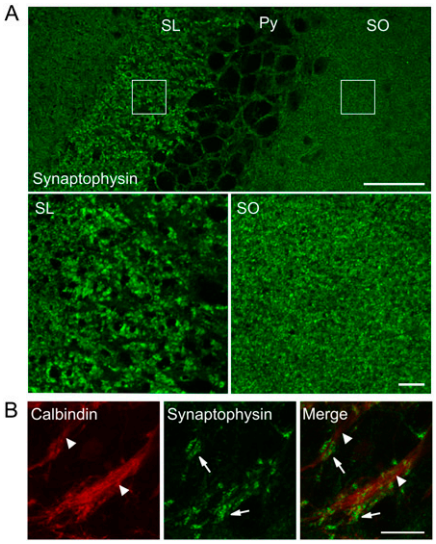

Fig. S8. Synaptophysin labeling in the CA3 and MFT. (*A*) Syaptophysin labeling in the stratum lucidum and stratum oriens of the CA3. *Lower Left* and *Lower Right* are enlargements of delineated areas in *Upper*. Note the size of MFT in the stratum lucidum compared with the labeling in the stratum oriens where no MFTs are found. (*B*) Synaptophysin labeling of the MFT. Calbindin (red) labeling MFs and synaptophysin (green) labeling MFTs in the proximal CA3. Note that synaptophysin is almost completely excluded from the fibers. MFs are labeled with arrows, and MFTs are labeled with arrowheads. Py, pyramidal cell layer; SL, stratum lucidum; SO, stratum oriens. (Scale bars: *A Upper*, 50 μm; *A Lower*, 10 μm; *B*, 20 μm.)